Available online at www.sciencedirect.com

ScienceDirect

Publishing Services by Elsevier

International Journal of Naval Architecture and Ocean Engineering 8 (2016) 235–242

http://www.journals.elsevier.com/international-journal-of-naval-architecture-and-ocean-engineering/

# Turbulence-induced noise of a submerged cylinder using a permeable FW–H method

Woen-Sug Choi [a,b], Yoseb Choi [a,b], Suk-Yoon Hong [a,b], Jee-Hun Song [c,*], Hyun-Wung Kwon [d], Chul-Min Jung [e]

[a] *Department of Naval Architecture and Ocean Engineering, Seoul National University, Seoul, South Korea*
[b] *Research Institute of Marine Systems Engineering, Seoul National University, Seoul, South Korea*
[c] *Department of Naval Architecture and Ocean Engineering, Chonnam National University, Yeosu, South Korea*
[d] *Department of Naval Architecture and Ocean Engineering, Koje College, Koje, South Korea*
[e] *The 6th R&D Institute-3rd Directorate, Agency for Defense Development, Changwon, South Korea*

Received 28 October 2015; revised 21 January 2016; accepted 8 March 2016
Available online 13 May 2016

**Abstract**

Among underwater noise sources around submerged bodies, turbulence-induced noise has not been well investigated because of the difficulty of predicting it. In computational aeroacoustics, a number of studies has been conducted using the Ffowcs Williams–Hawkings (FW–H) acoustic analogy without consideration of quadrupole source term due to the unacceptable calculation cost. In this paper, turbulence-induced noise is predicted, including that due to quadrupole sources, using a large eddy simulation (LES) turbulence model and a developed formulation of permeable FW–H method with an open source computational fluid dynamics (CFD) tool-kit. Noise around a circular cylinder is examined and the results of using the acoustic analogy method with and without quadrupole noise are compared, i.e. the FW–H method without quadrupole noise versus the permeable FW–H method that includes quadrupole sources. The usability of the permeable FW–H method for the prediction of turbulence-noise around submerged bodies is shown.


*Keywords:* Turbulence-induced noise; Circular cylinder; Acoustic analogy; Permeable FW–H method; OpenFOAM

## 1. Introduction

Future ships will be faster, bigger and more complex while satisfying ever-increasing demands for better acoustic performance. Accordingly, future hydrodynamic designs for ship hulls and appendages or other submerged bodies will have to meet higher acoustic requirements. Studies on hydrodynamic noise generated by such bodies have been mainly concentrated on the subject of the propeller and the propagation of sound, and have demonstrated limited understandings and predictability. However, noise generated by other underwater appendages underwater will increase as they become faster and larger. For appendages like a sonar dome, to maintain the performance so that it is not affected by its self-noise, it is important to be able to predict noise generated by vortex shedding, which involves non-linear quadrupole source noise. By correctly predicting such turbulence-induced noise, a designer can deal with the characteristics of flow noise at the design stage.

Objects in motion disturb the surrounding fluid to produce hydrodynamic noise. Such noise can be predicted using the Kirchhoff formula or acoustic analogy, which were developed for aero-acoustics (Lighthill, 1952; Ffowcs Williams and Hawkings, 1969; Wang et al., 2006). The acoustic analogy method has an advantage over the Kirchhoff formula due to its representation of noise in three source terms to which physical

* Corresponding author.
*E-mail address:* jhs@jnu.ac.kr (J.-H. Song).
Peer review under responsibility of Society of Naval Architects of Korea.

http://dx.doi.org/10.1016/j.ijnaoe.2016.03.002

meanings can be assigned: thickness noise, loading noise and quadrupole noise (Ffowcs Williams and Hawkings, 1969). Meanwhile, regarding far-field radiation noise, in order to reduce computational cost the turbulence-induced quadrupole noise term has usually been neglected. However, unlike the circumstances in air, it has recently been found that turbulence-induced quadrupole noise is also important for understanding the overall characteristics of far-field noise underwater (Ianniello et al., 2014b).

Pressure perturbations of the turbulence-induced noise can be predicted correctly using the Direct Numerical Simulation (DNS) method. However, it is almost impossible to use because of extremely high computational cost (Singer and Lockard, 2002; Inoue and Hatakeyama, 2002). Therefore, to reduce computational expense hybrid methods utilizing Cmputational Fuid Dynamics (CFD) with turbulent models and acoustic analogy methods introduced by Lighthill being actively studied (Wang et al., 2006). Based on Lighthill's analogy (Lighthill, 1952), Curle (1955) has improved the theory to consider a stationary boundary and Ffowcs Williams and Hawkings, (1969) have further developed the method to consider an object moving in arbitrary motion— the Ffowcs Williams–Hawkings (FW–H) analogy. The FW–H analogy was manipulated for computation as formulations 1 and 1A and further refined by Farassat (2007). For practical applications, formulation 1A is commonly used with neglect of the quadrupole noise source term (Wang et al., 2006; Farassat, 2007; Ansys, 2009).

The effort to calculate quadrupole noise has mainly focused on helicopter rotors in the supersonic region due to the associated dominance of quadrupole noise as formulation Q1A (Hanson and Fink, 1979; Farassat, 1987; Brentner, 1996; Brentner and Holland, 1997; Ianniello, 1998). However, while formulation Q1A includes a quadrupole noise term similar to that of formulation 1A that was to be introduced more than two decades later, the method is still underdeveloped and under researched, without ever having been studied for underwater circumstances (Di Francescantonio, 1997; Lockard and Casper, 2005).

In previous work, attempt to forcibly select permeable surface as wall surface condition for formulation 1A to see the effect of including quadrupole noise has been done using commercial software, Ansys FLUENT (Choi et al., 2015). The results was somehow meaningful yet, had no clear physical explanations of increase in sound pressure level using permeable surface. Also, unlike the cases in air, the proper results could only be obtained using reversed normal for underwater cases.

In this study, the use of a Large Eddy Simulation (LES) turbulence model of CFD and developed formulation of permeable FW–H method, which accommodates permeable surface, is shown to predict turbulence-induced noise without neglect of the quadrupole noise source terms. The developed solver, termed Ship NOise Field Operation And Manipulation (SNOFOAM), is based on the OpenFOAM platform, an object-oriented, open source CFD tool-kit (Jasak, 2009; Weller et al., 1998). SNOFOAM can be used as standard solver during the CFD calculation as well as for post-processing protocols to suit research objectives. For simplicity, noise around a circular cylinder is examined using two different methods: the commonly used FW–H method without a quadrupole noise source versus the developed formulation of permeable FW–H method that can take quadrupole noise sources into account.

## 2. Theoretical background

### 2.1. Governing equations and subgrid-scale modelling

Large eddy simulations are implemented in this research—for turbulence closure and to lend accuracy comparable to that of acoustic calculations (Wang et al., 2006; Batten et al., 2007). The use of LES to obtain noise predictions by integral solutions of the wave equation has been already used successfully in many previous works, for the high-Reynolds number range in the subcritical regime (Boudet et al., 2003; Takaishi et al., 2007; Kato et al., 2007). In the LES model, the large-scale motions are explicitly computed and for the system to be closed eddies within the scales of low-pass spatial filtering of the turbulent motions are modeled with subgrid-scale modelling (Sagaut, 2006).

The eddy-viscosity assumption is commonly used to model the Subgrid-Scale (SGS) tensor, $\tau_{ij} = \widetilde{u_i u_j} - \widetilde{u}_i \widetilde{u}_j$ in LES, for simplicity, as was begun by Smagorinsky (Pope, 2000; Sagaut, 2006). Here, $\widetilde{u}_i$ is the resolved velocity component in Cartesian coordinates ($i,j \in [1,2,3]$). The Smagorinsky model is based on the Boussinesq approximation, which represents the turbulence stresses as having linear behavior as represented by the large-scale strain rate tensor $S_{ij}$ (implicit summation rule for repeated indices is used and the tilde denotes the filtering operation)

$$\tau_{ij} - \frac{1}{3}\delta_{ij}\tau_{kk} = -2\upsilon_{sgs}\widetilde{S}_{ij} = -\upsilon_{sgs}\left(\frac{\partial \widetilde{u}_i}{\partial x_j} + \frac{\partial \widetilde{u}_j}{\partial x_i}\right) \tag{1}$$

where $\delta_{ij}$ denotes the Kronecker delta and $\upsilon_{sgs}$ is the subgrid-scale eddy viscosity. $S_{ij}$ is rate-of-strain tensor.

The SGS eddy viscosity, by a simple dimensional analysis, can be written as

$$\upsilon_{sgs} = l^2\left|\widetilde{S}_{ij}\right| = l^2\sqrt{2\widetilde{S}_{ij}\widetilde{S}_{ij}} \tag{2}$$

$$l = C_s\widetilde{\Delta} = C_s(\Delta x \Delta y \Delta z)^{1/3} \tag{3}$$

where $C_s$ is a constant and $\Delta$ is the filter width (the subgrid characteristic length-scale, the cell size in practice) and $l$ is a differential operator associated with the model for the resolved velocity field. The value of the constant $C_s$ is flow-dependent and found to vary from 0.065 to 0.25 and it is set to be $C_s = 0.2$ (Zhang et al., 2015). The filter width $\Delta$ is correlated to the typical grid spacing through the cube root of the cell volume.

### 2.2. Basic theory of acoustic analogy

Lighthill has introduced the wave equation of acoustic analogy, having the source derived by comparing the exact equations of motion of a fluid with the equations of sound propagation in a medium at rest as follows (Lighthill, 1952),

$$\frac{1}{c^2}\frac{\partial^2\rho'}{\partial^2 t}-\nabla^2\rho'=\frac{\partial^2 T_{ij}}{\partial x_i\partial x_j} \tag{4}$$

$$T_{ij}=\rho v_i v_j+p_{ij}-c^2\rho'\delta_{ij} \tag{5}$$

here $\rho'=\rho-\rho_0=$ density perturbation, $T_{ij}=$ Lighthill's stress tensor, $p_{ij}=$ compressive stress tensor, $c=$ velocity of sound in fluid at rest, $v_i=$ component of velocity in direction $x_i$.

Curle's analogy has expanded the Lighthill's theory by considering a rigid surface (Curle, 1955), and Ffowcs Williams and Hawkings have further generalized the theory by considering a rigid object in arbitrary motion as follows (Ffowcs Williams and Hawkings, 1969),

$$\left(\frac{\partial^2}{\partial t^2}-c^2\frac{\partial^2}{\partial x_i^2}\right)\rho'=\frac{\partial^2 T_{ij}}{\partial x_i x_j}-\frac{\partial}{\partial x_i}\left(P_{ij}\delta(f)\frac{\partial f}{\partial x_j}\right)+\frac{\partial}{\partial t}\left(\rho_0 v_i\delta(f)\frac{\partial f}{\partial x_i}\right) \tag{6}$$

where $f$ represents body surface as implicitly defined by the function $f(x,t)=0$; $f<0$ and $f>0$ meaning inside and outside of rigid body, respectively. The first term physically means unsteadiness inside the fluid expressed in the quadruple source term as a Reynolds stress and called the turbulence-induced noise term. The second term is a dipole source due to dilatation of boundaries and third term is monopole source modeled from fluctuating stresses on the surface. The second and third terms are called the loading noise and thickness noise terms, respectively.

Farassat's formulation 1A develops FW−H analogy equation into following integral forms (Farassat, 2007),

$$4\pi P_{Thickness}=\int_{f=0}\left[\frac{\rho_0\dot{v}_n}{r(1-M_r)^2}\frac{\rho_0 v_n\dot{\hat{r}}_i\dot{M}_i}{r(1-M_r)^3}\right]_{ret}dS+\int_{f=0}\left[\frac{\rho_0 c v_n(M_r-M^2)}{r^3(1-M_r)^3}\right]_{ret}dS \tag{7}$$

$$4\pi P_{Loading}=\int_{f=0}\left[\frac{\dot{p}cos\theta}{cr(1-M_r)^2}+\frac{\dot{\hat{r}}_i\dot{M}_i pcos\theta}{cr(1-M_r)^3}\right]_{ret}dS+\int_{f=0}\left[\frac{pcos\theta}{r^2(1-M_r)}+\frac{(M_r-M^2)pcos\theta}{r^2(1-M_r)^3}\right]_{ret}dS \tag{8}$$

$$4\pi P_{Quadrupole}=\frac{\partial^2}{\partial x_i x_j}\int_V\left[\frac{T_{ij}}{r|1-M_r|}\right]_{ret}dV \tag{9}$$

where $1-M_r$ is Doppler factor, $r=|x-y|$, and all terms evaluated in retarded time $t_{ret}=t-r/c$.

The turbulence term that is represented as a quadrupole source is a volume integration. Deciding upon the volumes in the fluid around rigid body over which to integrate and evaluate the integration kernel is difficult (Farassat and Brentner, 1988). The permeable FW−H method starts by establishing a permeable surface by doing away with the assumption of surface $f$ that the normal velocity of fluid ($v_n$) and the normal velocity of the rigid body ($u_n$) are equal ($v_n=u_n$); they are allowed to be unequal. By so, the calculation of thickness and loading noise on the permeable surface (control surface, computational surface, inner-cell) includes the turbulence-induced noise inside the surface (Wang et al., 2006; Farassat, 2007).

### 2.3. Development of formulation for the permeable FW−H method

The first-tried concept for treating quadrupole noise in the FW−H method was during the development of the Kirchhoff-FWH method, to take advantage of both the Kirchhoff method and FW−H method in prediction of hovering rotor noise (Di Francescantonio, 1997). To calculate the quadrupole term in the original FW−H method requires volume integration in the region around the body and control surface which has a high computational cost. Moreover, the difficulty of selecting an adequate region to perform the integration leads to uncertainty of accuracy and randomness in calculated results (Farassat and Brentner, 1998). To avoid those problems, following developed formulation takes advantage of the possibility of moving the control surface outward, so that the effect of the quadrupole noise sources within it can be accounted for by surface source terms.

Eq. (6) can be rearranged using mass-like flux $U_i$ , momentum flux $L_i$ and $f$ representing control surface.

$$\left(\frac{\partial^2}{\partial t^2}-c^2\frac{\partial^2}{\partial x_i^2}\right)\rho'=\frac{\partial^2 T_{ij}}{\partial x_i x_j}-\frac{\partial}{\partial x_i}[L_i\delta(f)|\nabla f|]+\frac{\partial}{\partial t}[\rho_0 U_n\delta(f)|\nabla f|] \tag{10}$$

$$U_i=u_i+[(\rho/\rho_0)-1](u_i-v_i), \tag{11}$$

$$L_{ij}=P_{ij}+\rho u_i(u_j-v_j) \tag{12}$$

here Reynolds stress tensor $T_{ij}$ is defined outside control surface:

$$T_{ij}=\rho u_i u_j+P_{ij}-c\rho'\delta_{ij} \tag{13}$$

by neglecting the quadrupole term with a simple dimensional comparison (Farassat, 1987), the solution of Eq. (10) using a Green's function

$$\rho' = -\frac{\partial}{\partial x_i}\int \frac{L_i\delta(f)\delta(g)|\nabla f|}{4\pi r}d^3y d\tau + \frac{\partial}{\partial t}\int \frac{\rho_0 U_n\delta(f)\delta(g)|\nabla f|}{4\pi r}d^3y d\tau \tag{14}$$

where $g = t-\tau-r/c$. Change of fixed coordinate system $y$ into moving coordinate system $\eta$ along with control surface Jacobian $J$

$$\rho' = -\frac{\partial}{\partial x_i}\int \frac{L_i\delta(f)\delta(g)|\nabla_y f|J}{4\pi r}d^3\eta d\tau + \frac{\partial}{\partial t}\int \frac{\rho_0 U_n\delta(f)\delta(g)|\nabla_y f|J}{4\pi r}d^3\eta d\tau \tag{15}$$

The Eq. (15) shows general form of the permeable FW−H equation. Eq. (15) can also be written in a retarded time formulation considering integration by $\tau$ in time with no change in the control surface $\delta(f)$.

$$\rho' = -\frac{\partial}{\partial x_i}\int \left[\frac{L_i\Lambda}{4\pi r|1-M_r|}\right]_{ret} dS(\eta) + \frac{\partial}{\partial t}\int \left[\frac{\rho_0 U_n\Lambda}{4\pi r|1-M_r|}\right]_{ret} dS(\eta) \tag{16}$$

here $\Lambda = J|\nabla_y f|/|\nabla_\eta f| =$ ratio of area elements in $\eta$ and $y$ spaces. If the control surface is undistorted in motion, $\Lambda = 1$.Since,

$$-\frac{\partial}{\partial x_i}\int \left[\frac{Q_i}{r|1-M_r|}\right]_{ret} dS = \frac{\partial}{\partial t}\int \left[\frac{Q_i r_i}{cr^2|1-M_r|}\right]_{ret} dS + \int \left[\frac{Q_i r_i}{r^3|1-M_r|}\right]_{ret} dS \tag{17}$$

$$\frac{\partial[Q(\tau)]_{ret}}{\partial t} = \left[\frac{1}{(1-M_r)}\frac{\partial Q(\tau)}{\partial \tau}\right]_{ret} \tag{18}$$

leads to the formulation of permeable FW−H method in surface integral form,

$$4\pi P_{permeable\ FW-H} = \int_S \left[\frac{\dot{U}_n+\dot{U}_r}{r(1-M_r)^2}\right]_{ret} dS(\eta) + \int_S \left[\frac{\rho u_n\{r\dot{M}+c(M_r-M^2)\}}{r^2(1-M_r)^3}\right]_{ret} dS(\eta) + \int_S \left[\frac{\dot{L}_r}{cr(1-M_r)^2}\right]_{ret} dS(\eta) + \int_S \left[\frac{L_r-M_r}{r^2(1-M_r)^3}\right]_{ret} dS(\eta) + \int_S \left[\frac{L_r\left\{r\dot{M}_r+c(M_r-M^2)\right\}}{cr^2(1-M_r)^3}\right]_{ret} dS(\eta) \tag{19}$$

Developed formulation only includes surface integration at the permeable surface with the moving coordinate system ($\eta$). The form not only has advantage in calculation cost, but also in straightforward applicability for computer codes.

For a relatively stationary body with an observer position, the Eq. (19) can be simplified as

$$4\pi P_{permeable\ FW-H} = \int_{f=0}\left[\frac{\rho\dot{u}_n n_i}{r}\right]_{ret} dS + \int_{f=0}\left[\frac{\dot{p}cos\theta+\rho\dot{u}_n u_r+\rho u_n\dot{u}_r}{cr}\right]_{ret} dS + \int_{f=0}\left[\frac{pcos\theta+\rho u_n u_r}{r^2}\right]_{ret} dS \tag{20}$$

here θ represents angle between direction of the flow and the receiver from axis of circular cylinder.

Also, Eqs. (7)–(9) can be simplified for a relatively stationary body by considering a surface integral on the surface defined by $v = 0$ as follows

$$4\pi P_{FW-H\ without\ Quad.} = \frac{1}{c}\int_{f=0}\left[\frac{\dot{p}cos\theta}{r}\right]_{ret} dS + \int_{f=0}\left[\frac{pcos\theta}{r^2}\right]_{ret} dS \tag{21}$$

Taking the difference between Eqs. (20) and (21) leaves the noise sources originating from the quadrupole noise term (Eq. (9)) of the original FW−H method. The result can be written as

$$4\pi P_{Quadrupole\ noise} = \int_{f=0} \left[\frac{\rho \dot{u}_n n_i}{r}\right]_{ret} dS + \int_{f=0} \left[\frac{\rho u_i u_j n_j \hat{r}_i}{r^2}\right]_{ret} dS + \int_{f=0} \left[\frac{\rho\left(\dot{u}_n u_r + \rho u_n \dot{u}_r\right) n_i \hat{r}_i}{cr}\right]_{ret} dS \quad (22)$$

Considering its physical meanings, the three source terms in Eq. (22) can be named, in order, the turbulence self-noise term, the turbulence generation term and the turbulence energy term. Such novel naming of each terms can be justified since each noise sources are produced due to velocity perturbation, Reynolds stress and turbulence energy perturbation.

## 3. Noise analysis of a cylinder

The procedure of noise analysis for a circular cylinder can be represented in four steps as in Fig. 1. Various standard solvers provided by OpenFOAM have been utilized inside SNOFOAM for calculations to stabilize the CFD calculations in preparation for the subsequent acoustical calculation.

### 3.1. Construction of mesh

To analyze a cylinder of 20 mm in diameter, a total of 3.6 million unit volume cells are constructed. Overall, the mesh takes on an O-type shape, for better quality, such as skewness and orthogonality around the cylinder as shown in Fig. 2. The outer radius of the computational domain is 500 mm. The boundary condition for the left half of the outer radius is set to the velocity inlet while right half is set to the pressure outlet and a no slip condition is applied for the cylinder. Receiver points for the acoustic analysis are placed perpendicular to the flow direction downward from the cylinder at distances of 100 mm, 200 mm, 300 mm, 400 mm and 500 mm. The dimensionless wall distance (wall Y+) is set to lower than 1, to accurately calculate boundary layers.

### 3.2. Simulation of turbulent flow

OpenFOAM provides several standard solvers for incompressible flow. As it is often the case for the simulation of flows around bluff bodies, a steady-state solver was first performed followed by transient solvers for acoustic calculations. Standard solvers simpleFoam and pisoFoam were implemented inside SNOFOAM for steady-state solutions and transient solutions, respectively. The solver simpleFoam is a steady-state solver for compressible, turbulent flow while

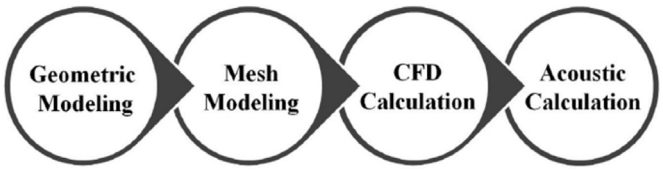


Fig. 1. Flow chart of hydrodynamic noise calculation.

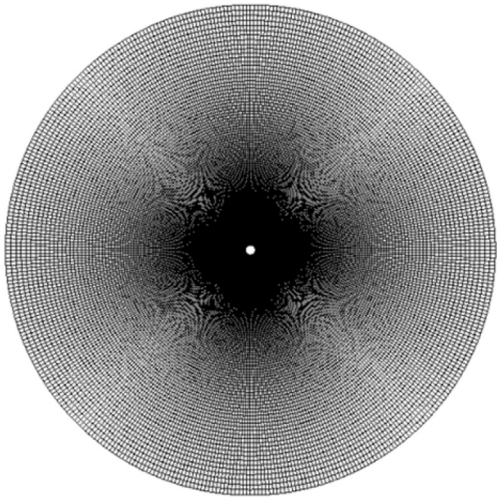

Fig. 2. View of the bottom grid surface, 3.6 million volumes cells (hexahedral type mesh).

pisoFoam is a transient solver for incompressible flow with generic turbulence modeling such as, laminar, Reynolds Averaged Navier Stokes equation (RANS) and LES. The usage of pisoFoam, the incompressible solver, can be justified due to its incompressibility for underwater environment. Also, it is inevitable to perform transient calculations in order to accumulate flow data at each time steps for acoustic calculations.

Incompressible Navier–Stokes equations are solved using a finite volume method along with a linear reconstruction scheme, to allow the use of constructed meshes of arbitrary shapes. The "Pressure Implicit with Splitting of Operators" (PISO) algorithm is used for the pressure–velocity coupling. Time derivatives were discretized by the bounded second-order Crank-Nicolson scheme to sufficiently resolve fluctuations for the acoustic calculations. The spatial schemes for the interpolation, the gradient, the Laplacian and the divergence terms are linear, Gauss linear, Gauss linear corrected and Gauss linear, respectively. The settings for the CFD calculations were referenced by Zhang et al. (2015), and further details of the schemes are in OpenFOAM guide.

The results are shown in Figs. 3 and 4. To verify the flow simulation, the results are compared with the reference with the same Reynolds number, $Re = 9 \times 10^4$. Figs. 3 and 4 shows flow simulation results for the dynamic pressure and pressure coefficient. Fig. 4 shows good agreement with the reference

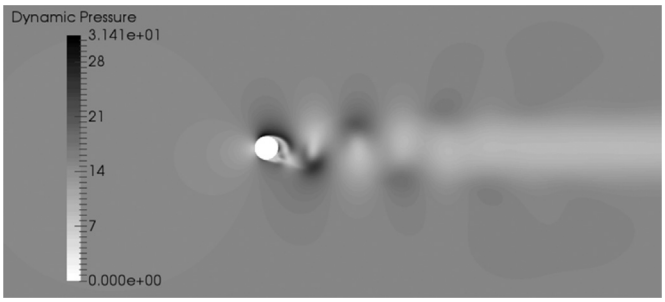


Fig. 3. Dynamic pressure contour around a cylinder.

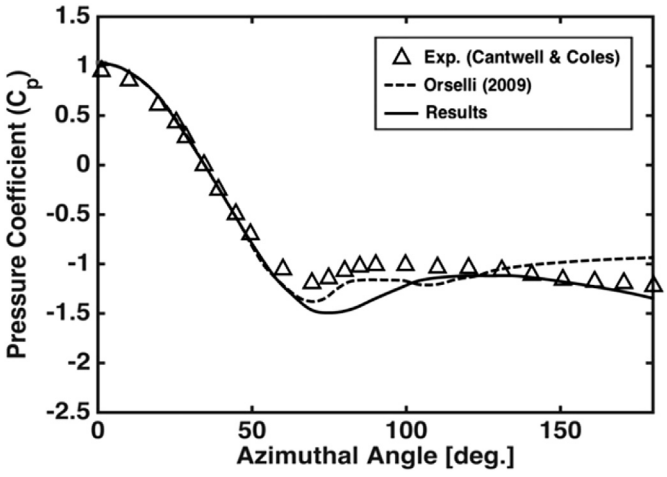


Fig. 4. Pressure coefficient around a cylinder.

(Orselli et al., 2009). In Table 1, it is verified that the Strouhal number of the simulation compares well with that of references (Orselli et al., 2009; Park, 2012).

### 3.3. Turbulence-induced noise analysis

It is often the case with applications of the FW−H method to neglect the quadrupole noise source because of the high computational cost that is caused by the volume integral. As was derived in Theoretical Background section, the permeable FW−H method avoids such calculations so as to have a similar calculation time as that of the commonly used FW−H method that neglects the quadrupole source. The estimated calculation time for each receiver point by using SNOFOAM's post-processing utilities after the CFD calculation was about 8 h, with a common PC. Here, the time was mainly consumed by reading the previously saved data, which step is usually inevitable as the entire CFD data must be loaded into RAM (random access memory).

Novel comparisons of the predicted noise received at the designated receiver points around the cylinder at $\mathrm{Re} = 9 \times 10^4$ in an underwater environment are shown in Fig. 5. The permeable surface, where the computation of the permeable FW−H method is being done, is set with a radius of 50 mm. The criteria to set the size of the permeable surfaces need more investigation. From our experiences, setting the surface to include 3 to 5 vortex eddies up to staggered vortex steer emerge is suggested considering accuracy and calculation cost. Overall frequency characteristics of both the FW−H method without a quadrupole noise source and the permeable FW−H method showed similar results throughout the receiver points with stationary peak frequencies which well corresponds to the common results of cylinders in air in other simulations and experiments (Hong and Choi, 1998; Boudet et al., 2003; Orselli et al., 2009; Ianniello et al., 2014a, 2014b, 2014c; Cantweell and Cole, 1983). However, the results obtained by permeable FW−H method have more peaking frequencies compared to the other method.

Table 1
Comparison of the Strouhal number.

| Strouhal number ($S_t$) | |
|---|---|
| Experiment (Park, 2012) | 0.195 |
| Experiment (Norberg, 2003) | 0.190 |
| Simulations (Park, 2012) | 0.198 |
| Simulations (Orselli et al., 2009) | 0.191 |
| Result | 0.190 |

Analysis results in various receiver positions shows similar frequency characteristics with decrease in magnitude as distance increases. Unlike the calculation results of previous case (Choi et al., 2015), the receivers inside the permeable surface also shows the similar characteristics. It is due to the BEM (Boundary Element Method)-like concept being imposed using green's function on development of the permeable FW−H equations. Such results can be justified noting the fact that the pseudo-sound region(near-field) in air for cylinders are 5 times the diameter (Blevins, 1990) and it is smaller in underwater environment due to faster sound speed.

The difference between the two methods represents the effect of quadrupole noise, as was theoretically examined in previous section. Comparing the magnitudes of the sources in Eq. (22), the turbulence self-noise is dominant compared to the other two sources, turbulence production noise and turbulence energy noise. This implies that the turbulence-induced noise is mainly caused by eddies fluctuating in the wake of the cylinder compared to the noise radiated from the surface of the cylinder. Considering that, the gap between the two methods can be narrowed by reducing the sizes of the shed vortices by having a more slender airfoil-like shape.

The average gap in magnitude between the two methods is about 5 dB at the primary peak by considering the turbulence-induced noise. Moreover, apart from average magnitude differences, a notable difference between the predicted results of the two different methods is that the first few even ordered peaks, i.e. secondary, 4th and 6th, which is almost neglected in the results of the FW−H method without quadrupole noise, is more accurately predicted by the permeable FW−H method. It can be said that the frequency characteristics of turbulence-induced noise come to the fore at those peaks, compared to thickness noise and loading noise. Such observed results are rather novel in underwater environment and no such characteristics are reported in the references of results pertaining to the air environment.

## 4. Conclusions

A novel prediction of turbulence-induced noise around a circular cylinder in an underwater environment is done by two different methods: FW−H without a quadrupole noise source term, which is common for FW−H method applications in order to reduce computational cost; and, the developed formulation of permeable FW−H method using a permeable surface that includes turbulence-induced noise sources enclosed within the surface. Presenting no difference in calculation time, the developed formulation of permeable

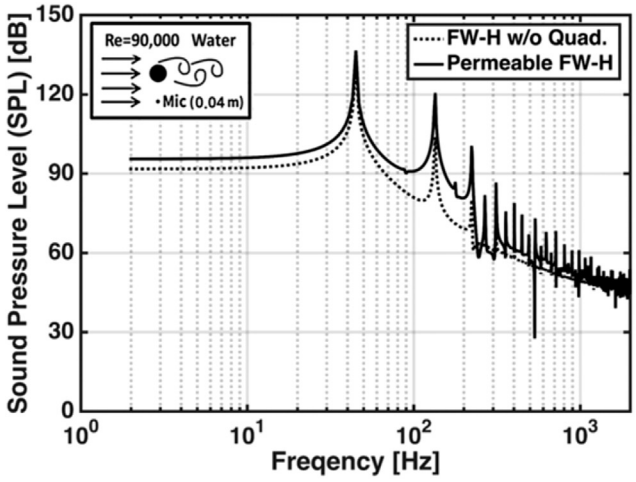


(a) : Receiver 1 (40 mm)

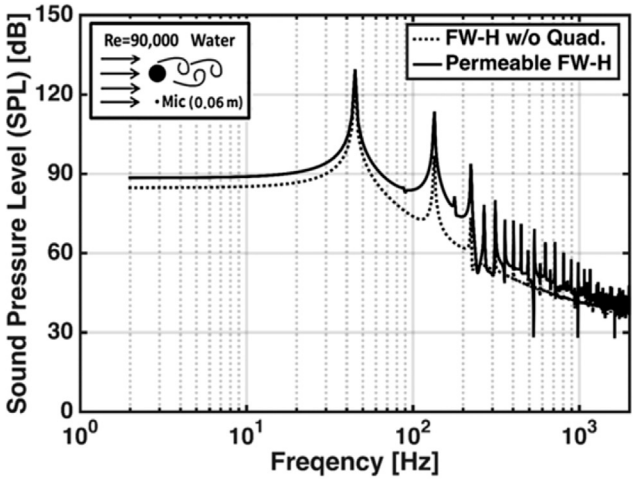


(b) : Receiver 2 (60 mm)

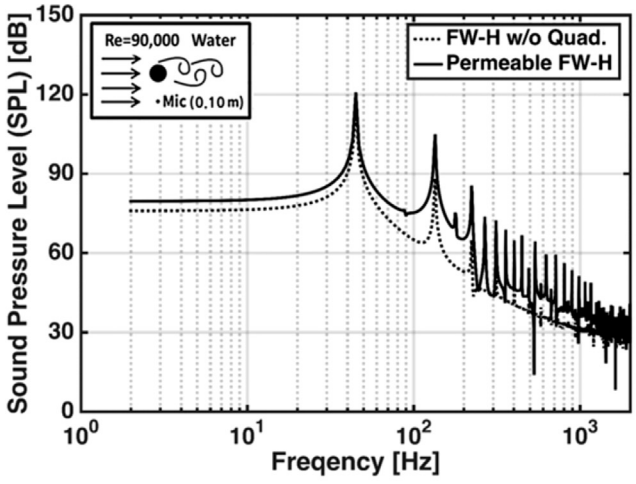


(c) : Receiver 3 (100 mm)

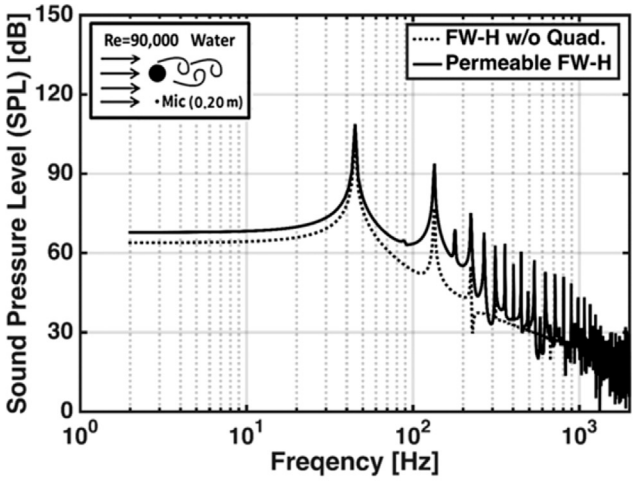


(d) : Receiver 4 (200 mm)

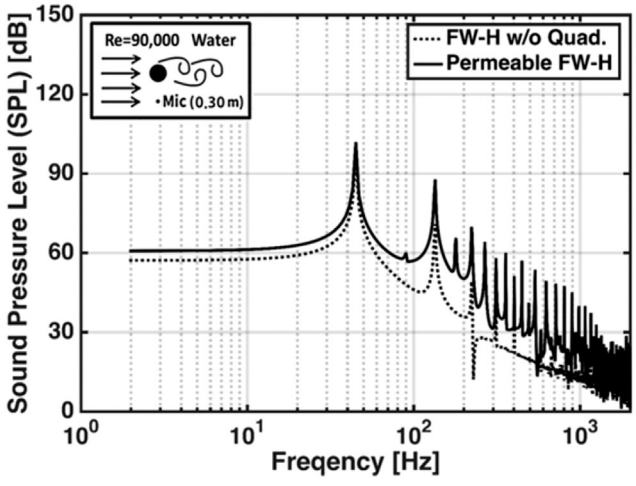


(e) : Receiver 3 (300 mm)

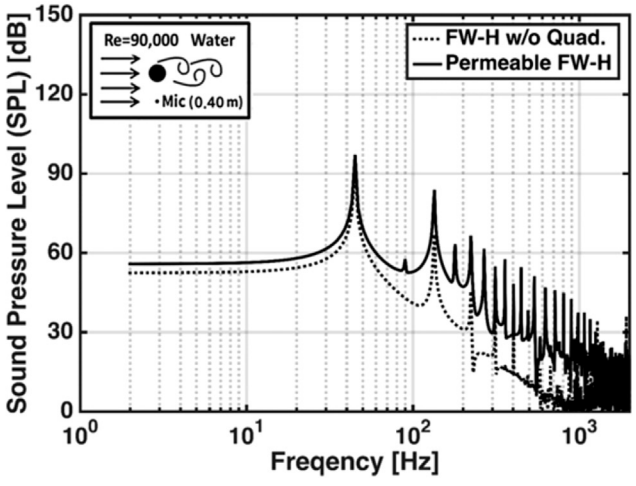


(f) : Receiver 4 (400 mm)

Fig. 5. Comparisons of sound pressure level spectrum underwater obtained from different method at Re = $9 \times 10^4$: (a) Receiver 1 (40 mm), (b) Receiver 2 (60 mm), (c) Receiver 3 (100 mm), (d) Receiver 4 (200 mm), (e) Receiver 5 (300 mm) and (f) Receiver 5 (400 mm).

FW–H method predicted the noise around cylinder well, matching commonly known frequency characteristics.

The differences between the FW–H method without a quadrupole source and the permeable FW–H method in representing the magnitude of the noise due to the quadrupole source was theoretically examined. The difference was mainly caused by the self-noise of eddies in vortex shedding, which led to an average magnitude difference of 5 dB at the primary peak as well as in the overall frequency range. Also, the results show that the secondary peak is mainly caused by the quadrupole source compared to the other sources in the original FW–H method. In conclusion, by comparing the two different methods, the usefulness of the permeable FW–H method for underwater environment is shown and novel characteristics are observed.

In further studies, the selection of the permeable surface for the permeable FW–H method will consider not only the size of the surface but also the length and frequency of vortex shedding. Turbulence-induced noise prediction in more complex geometries will be considered, to better understand the general features of predicting turbulence-induced noise in an underwater environment.

## Acknowledgments

This research was funded by Advanced Naval Vessels Research Laboratory, Seoul National University, Seoul, Korea. Also, supported by Research Institute of Marine Systems Engineering and Basic Science Research Program through the National Research Foundation of Korea (NRF) funded by Ministry of Education, Science and Technology (2011-0023027, 2012R1A1A22004034).

## References

Ansys, 2009. Ansys Fluent 12.0 Theory Guide Chapter 14. Aerodynamically Generated Noise, pp. 421–432.

Batten, P., Spalart, P., Terracol, M., 2007. Use of hybrid RANS/LES for acoustic source predictions. In: Large-eddy Simulation for Acoustics. Cambridge Aerospace Series. Cambridge University Press.

Blevins, R.D., 1990. Flow-induced Vibration, second ed. Van Nostrand Reinhold.

Boudet, J., Casalino, D., Jacob, M.C., Ferrand, P., 2003. Prediction of Sound Radiated by a Rod Using Large Eddy Simulation. AIAA, pp. 2003–3217.

Brentner, K.S., 1996. An Efficient and Robust Method for Predicting Helicopter Rotor High-speed Impulsive Noise. AIAA, pp. 96–0151.

Brentner, K.S., Holland, P.C., 1997. An efficient and robust method for computing quadrupole noise. J. Am. Helicopter Soc. 42, 172–181.

Cantwell, B., Coles, D., 1983. An experimental study of entrainment and transport in the turbulent near wake of a circular cylinder. J. Fluid Mech. 136, 321–374.

Choi, W., Hong, S., Song, J., Kwon, H., Jung, C., Kim, T., 2015. Turbulent-induced noise around a circular cylinder using permeable FW-H method. J. Appl. Math. Phys. 3, 161–165.

Curle, N., 1955. The influence of solid boundaries upon aerodynamic sound. Proc. R. Soc. Lond. A 231 (1187), 505–514.

Farassat, F., 1987. Quadrupole Source in Prediction of Noise of Rotating Blades-A New Source Description. AIAA Paper 87–2675.

Farassat, F., 2007. Derivation of Formulations 1 and 1A of Farassat. NASA/TM-2007–214853. NASA.

Farassat, F., Brentner, K.S., 1988. The uses and abuses of the acoustic analogy in helicopter rotor noise prediction. J. Am. Helicopter Soc. 33, 29–36.

Farassat, F., Brentner, K.S., 1998. Supersonic quadrupole noise theory for high-speed helicopter rotors. J. Sound Vib. 218 (3), 481–500.

Ffowcs Williams, J.E., Hawkings, D.L., 1969. Sound generation by turbulence and surfaces in arbitrary motion. Philos. Trans. R. Soc. Lond. A 264 (1151), 321–342.

Di Francescantonio, D., 1997. A new boundary integral formulation for the prediction of sound radiation. J. Sound Vib. 202 (4), 491–509.

Hanson, D.B., Fink, M.R., 1979. The importance of quadrupole sources in prediction of transonic tip speed propeller noise. J. Sound Vib. 62, 19–38.

Hong, H.B., Choi, J.S., 1998. Experimental study on the vortex-shedding sound from a yawed circular cylinder. J. Acoust. Soc. Am. 103 (5), 1937–1938.

Ianniello, S., 1998. Quadrupole Noise Predictions through the FW-H Equation. AIAA 98–2377.

Ianniello, S., Muscari, R., Di mascio, A., 2014a. Ship underwater noise assessment by the acoustic analogy, part I: nonlinear analysis of a marine propeller in a uniform flow. J. Mar. Sci. Technol. 18, 547–570.

Ianniello, S., Muscari, R., Di mascio, A., 2014b. Ship underwater noise assessment by the acoustic analogy, part II: hydroacoustic analysis of a ship scaled model. J. Mar. Sci. Technol. 19, 52–74.

Ianniello, S., Muscari, R., Di mascio, A., 2014c. Ship underwater noise assessment by the acoustic analogy, part III: measurements versus numerical predictions on a full-scale ship. J. Mar. Sci. Technol. 19, 125–142.

Inoue, O., Hatakeyama, N., 2002. Sound generation by a two-dimensional circular cylinder in a uniform flow. J. Fluid Mech. 471, 285–314.

Jasak, H., 2009. OpenFOAM: open source CFD in research and industry. Int. J. Nav. Archit. Ocean Eng. 1, 89–94.

Kato, C., Yamade, Y., Wang, H., Guo, Y., Miyazawa, M., Takaishi, T., Yoshimura, S., Takano, Y., 2007. Numerical prediction of sound generated from flows with a low Mach number. Comput. Fluids Chall. Adv. Flow Simul. Model. 36, 53–68.

Lighthill, M.J., 1952. On sound generated aerodynamically, I: general theory. Proc. R. Soc. A221, 564–587.

Lockard, D.P., Casper, J.H., 2005. Permeable Surface Corrections for Ffowcs Williams and Hawkings Integrals. AIAA, 2005–2995.

Norberg, C., 2003. Fluctuating lift on a circular cylinder: review and new measurement. J. Fluids Struct. 17 (1), 57–96.

Orselli, R.M., Meneghini, J.R., Saltra, F., 2009. Two and Three-dimensional Simulation of Sound Generated by Flow Around a Circular Cylinder. American Institute of Aeronautics and Astronautics, AIAA, pp. 2009–3270.

Park, I.C., 2012. 2-Dimensional Simulation of Flow-induced Noise Around Circular Cylinder. Theses and Dissertations. Chungnam University.

Pope, S.B., 2000. Turbulent Flows. Cambridge University Press.

Sagaut, P., 2006. Large Eddy Simulation for Incompressible Flows: an Introduction. Springer Science & Business Media.

Singer, B.A., Lockard, D.P., 2002. Hybrid acoustic predictions. Comput. Math. Appl. 46, 647–669.

Takaishi, T., Miyazawa, M., Kato, C., 2007. A computational method of evaluating noncompact sound based on vortex sound theory. J. Acoust. Soc. Am. 121, 1353–1361.

Wang, M., Freund, J.B., Lele, S.K., 2006. Computational prediction of flow-generated sound. Annu. Rev. Fluid Mech. 38, 483–512.

Weller, H.G., Tabor, G., Jasak, H., Fureby, C., 1998. A tensorial approach to computational continuum mechanics using object-oriented techniques. Comput. Phys. 12 (6), 620–631.

Zhang, H., Yang, J., Xiao, L., Lu, H., 2015. Large-eddy simulation of the flow past both finite and infinite circular cylinders at Re = 3900. J. Hydrodyn. Ser. B 27, 195–203.